PCCP

Accepted Manuscript

ROYAL SOCIETY OF CHEMISTRY

www.rsc.org/pccp

Direct Measurements of the Interactions between Clathrate Hydrate Particles and Water Droplets

Chenwei Liu[a,b] *, Mingzhong Li*[a]*, Guodong Zhang*[a]*， Carolyn A. Koh**[b]

[a] *College of Petroleum Engineering, China University of Petroleum, Qingdao 266580, China*

[b]*Center for Hydrate Research, Chemical & Biological Engineering Department, Colorado School of Mines, Golden, CO 80401, USA*

Abstract

Clathrate hydrate particle agglomeration is often considered to be one of the key limiting factors in plug formation. The hydrate particle–water interaction can play a critical role in describing hydrate agglomeration, yet is severely underexplored. Therefore，this work investigates the interactions between water droplets and cyclopentane hydrate particles using a Micromechanical Force (MMF) apparatus. Specifically, the effect of contact time, temperature/subcooling, contact area, and the addition of Sorbitane monooleate (Span 80) surfactant on the water droplet–hydrate particle interaction behavior are studied. The measurements indicate that hydrate formation during the measurement would increase the water-hydrate interaction force significantly. The results also indicate that the contact time, subcooling and concentration of cyclopentane, which determine the hydrate formation rate and hydrate amount, will affect the hydrate-water interaction force. In addition, the interaction forces also increase with the water-hydrate contact area. The addition of Span 80 surfactant induces a change in the hydrate morphology and renders the interfaces stable versus unstable (leading to coalescence), and the contact force can affect the hydrate-water interaction behavior significantly. Compared with the hydrate-hydrate cohesion force (measured in cyclopentane), the hydrate-water adhesion force is an order of magnitude larger. These new measurements can help to provide new and critical insights into the hydrate agglomeration process and potential strategies to control this process.

Keywords: hydrate, agglomeration, interaction force, contact time, Micromechanical Force, surfactant

Introduction

Gas clathrate hydrates are crystalline inclusion compounds comprised of hydrogen bonded water cavities, which encapsulate suitably sized gas molecules at high pressures and low temperatures. The high pressure and low temperature in oil and gas production pipelines provide favorable conditions for gas hydrate formation [1]. The aggregation and accumulation (or bedding) of hydrates in pipelines can lead to pipeline blockage, resulting in catastrophic operational failures and safety hazards to personnel and equipment [1,2]. As gas and oil exploration and production move to ultradeep water (>8000 ft of sea water), the risk of hydrate formation increases significantly and is considered to be a major flow assurance (i.e. maintaining flow in the pipeline) challenge in oil and gas pipelines [1].

For the oil-dominated pipeline system under flow, water can be dispersed into the oil phase, creating a water-in-oil (W/O) emulsion [3]. Over the past decade, a four step conceptual model (Fig. 1) that depicts hydrate plug formation in W/O emulsions has been developed and gained acceptance within the flow assurance community [4]. These four steps to plug formation include: (i) water entrainment in the oil phase, (ii) hydrate shell growth at the water−oil interface, (iii) hydrate aggregation, and (iv) accumulation/plugging of hydrate particles and aggregates. This conceptual picture suggests that hydrate agglomeration is a key limiting factor in plug formation [1]. Specifically, Fidel-Dufour [5] proposed a conceptual mechanism for agglomeration, which suggests that the interactions between unconverted water droplets and hydrate particles will play an important role at the early stage of the agglomeration. The hydrate agglomeration process could be considered as analogous to the wet granulation process. The wet granulation process refers to the process of adding a liquid solution/binder to powders, forming bonds between powdered particles [6]. The granulation process is usually regarded as a combination of three sets of rate processes [7,8]: (i) wetting and nucleation, where the liquid binder is brought into contact with a dry powder bed,

to give a distribution of nuclei/granules, (ii) consolidation and growth, where collisions between two granules, granules and feed powder lead to granule compaction and growth; and (iii) attrition and breakage, where wet or dry granules break due to impact, wear or compaction in the granulator. In oil and gas pipelines, when some water droplets are converted into hydrate particles, as expected, the residual unconverted droplets can serve as the added liquid solution/binder, while the water-wet hydrate particles will play the role of powders in wet granulation. Subsequently, larger sized hydrate agglomeration could be formed after the three sets of rate processes. Therefore, the interactions between a liquid droplet and a solid particle should play a critical role in describing granulation/agglomeration. Multiple studies to-date have focused on hydrate–hydrate particle interaction [9-13]. In contrast, reported work on the interactions between water droplets and hydrate particles is limited [14-16].

This work aims to investigate the interaction between water droplets and cyclopentane hydrate particles using a Micromechanical Force (MMF) apparatus. Specifically, we studied the effect of contact time, temperature/ subcooling ($\Delta T_{sub} = T_{eqm} - T_{expt}$), contact area, and the addition of mineral oil and Span 80 on the water droplet–hydrate particle interaction. The measurements and observations can provide new insights into the hydrate agglomeration process.

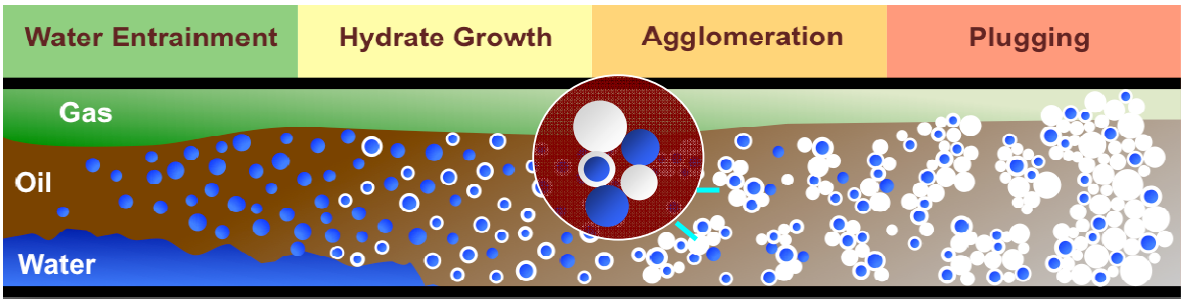

Fig. 1 Conceptual picture for hydrate formation in oil-dominated systems. (Modified from D. Turner [3] & J. Abrahamson).

Experimental

Chemicals

Cyclopentane (CyC5) hydrate forms at atmospheric pressure, with a dissociation temperature of 7.7 ºC [1]. Cyclopentane is immiscible in water and forms structure II hydrate, which is the structure usually encountered in petroleum fields [1]. Cyclopentane hydrate therefore serves as an atmospheric pressure model hydrate former and is thus suitable for laboratory experiments without pressurized equipment. The cyclopentane (98 % purity) used in this work is from Fisher Scientific. Sorbitane monooleate, Span 80 (MW 428.61 g/mol, Sigma Aldrich) is a surfactant with a hydrophillic-lipophilic balance (HLB) value of 4.3, which is usually used to produce water-in-oil emulsions [3]. Crystal Plus mineral oil 70T (STE Oil Company, Inc.) has a density of 0.857 g/cm^3 at 20 ºC and the gas chromatography compositional analysis of mineral oil 70T is listed in Table 1[3]. The estimated average molecular weight of mineral oil 70T is about 311g/mol.

Table 1. Composition of mineral oil 70T

Component	Molecular weight g/mol	Density g/ml	Mass %	Component	Molecular weight g/mol	Density g/ml	Mass %
n-C_{16}	226	0.773	0.09	n-C_{24}	338	0.797	4.23
n-C_{17}	240	0.777	1.23	n-C_{25}	352	0.801	3.76
n-C_{18}	254	0.777	5.22	n-C_{26}	366	0.778	3.29
n-C_{19}	268	0.786	11.75	n-C_{27}	380	0.780	2.66
n-C_{20}	282	0.789	16.04	n-C_{28}	394	0.807	2.27
n-C_{21}	296	0.792	17.04	n-C_{29}	408	0.808	1.56
n-C_{22}	310	0.778	12.20	n-C_{30}^+	422	0.810	12.34
n-C_{23}	324	0.797	6.34				

Water droplet and CyC5 hydrate particle measurements

A micromechanical force (MMF) apparatus was used for measuring the interaction between a water droplet and CyC5 hydrate particle. The MMF system has been extensively discussed in our previous work to measure the interaction force between hydrate-hydrate [9] and hydrate-substrate [17-18] systems. The MMF apparatus consists of a Zeiss S100 inverted light microscope, placed on a vibration isolation table and encased in a dry box. The microscope stage holds an aluminum cell which is surrounded by a cooling jacket connected to an external

refrigeration unit (1196D, VWR International, Inc.) which recirculates an ethylene glycol/water mixture to/from the cell (Fig. 2). A circular cover glass was placed on the bottom of the cell to allow for visualization. The experimental cell was filled with liquid cyclopentane and housed two cantilevers. The left-hand cantilever was connected to a manual micromanipulator, while the right-hand cantilever was connected to a remotely operated micromanipulator (Eppendorf Patchman 5173). At the end of the right hand cantilever, an aluminum plate (EN AW 5052), polished using 400 grit sanding sheets abrasive material (MSC industrial supply Co.), was fixed to place the water droplet onto it. The method of placing fluid droplets or gas bubbles on flat plates has been widely used in other applications for particle-droplet/particle-bubble interaction measurements [14-16,19-22]. Prior to the experiments, the aluminum plate was rinsed with distilled water, acetone, ethanol and finally dried using a heat gun.

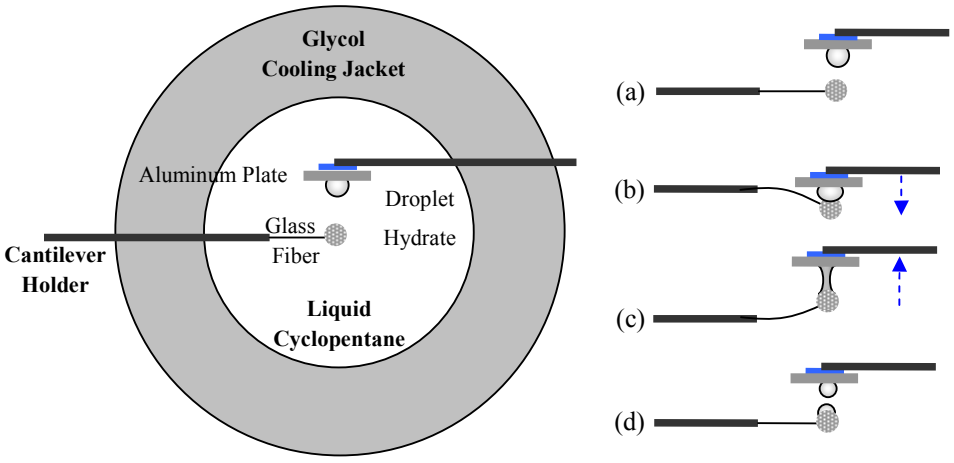

Fig. 2 Top view of the experimental cell setup for hydrate-droplet interaction measurements (left) and the sequence of steps in the measurements (right).

In the measurements, a dropper was used to place a drop of deionized water on the end of the left-hand glass fiber cantilever. The droplet was quenched in liquid nitrogen for 20 s to completely convert the water to ice. The ice

particle was placed immediately in the cyclopentane bath (maintained at 268 K). The liquid CyC5 temperature was then slowly raised above the ice freezing temperature, allowing the ice particle to convert to a cyclopentane hydrate particle [9] with an approximate radius of 329±21μm. At the experimental temperature, the right-hand cantilever was first immersed in the CyC5 cell for 30 minutes. The same dropper technique was used again to form another water drop on the end of another glass fiber (spare) cantilever. The water droplet was then transferred from the glass fiber (spare) cantilever to the aluminum plate immersed in the CyC5 cell. The equivalent radius of the droplet on the plate was about 259±13μm. After a 30 minutes equilibration period, the MMF measurements were performed and the hydrate particle (on the left hand cantilever) appeared to be completely rigid. The measurements procedure included "approaching" and "retracting" periods (illustrated in Fig. 2). During the approaching period, the droplet was slowly brought into contact with the hydrate particle, creating a preload force on the hydrate particle due to bending of the left-hand cantilever (Fig. 2 (a) and (b)). While "retracting", the droplet moves away from the hydrate particle slowly until the droplet-hydrate particle is detached (Fig. 2 (c) and (d)). The approaching and retracting velocities of the plate were determined to be around 7 to 9 μm/s to eliminate the interference of hydrodynamics on the measurement. Unless specified otherwise, no residence time is allowed before the retracting period.

The displacement of the left-hand cantilever during the measurement was captured in real-time with 30 frames per second. The displacement was multiplied by the cantilever spring constant (i.e., Hooke's law) to estimate the interaction force between the water droplet and hydrate particle. In all the measurements, a positive displacement indicates a downward deflection of the hydrate particle cantilever from its free position, and hence represents a repulsive force between the hydrate particle and droplet. A negative displacement involves pulling up the cantilever and hence represents an attractive force.

Results and discussion

Effect of contact time

The interaction force of a water droplet approaching and retracting from a hydrate particle in pure CyC5 at 1.5 ºC (i.e. at a subcooling of 6.2 ºC, see Fig. S1) as a function of aluminum plate displacement is shown in Fig. 3, together with the respective microscope images. As the aluminum plate approaches the hydrate particle at a constant velocity from position I, the distance between the water droplet and hydrate particle decreases. There is no measurable net interaction force acting upon the two surfaces until point II at which point the hydrate particle is rapidly drawn into the water droplet. The hydrate-CyC5-water three phase contact (TPC) line forms and can expand on the hydrate particle surface instantaneously. This phenomenon can be explained in terms of surface energy, where the system tends to reduce its interfacial Gibbs free energy to an equilibrium state. Cyclopentane hydrate is water-wet, and the interfacial tension between water and cyclopentane hydrate is about 0.32±0.05mN/m [23]. The interfacial tension of hydrate-CyC5 and water-CyC5 is estimated at 47±0.05mN/m [23] and 48.72mN/m [24], respectively. The initial contact of water with a hydrate particle will create a new hydrate-water interface with lower interfacial tension, and meanwhile reduce the hydrate-CyC5 and water-CyC5 interface with high interfacial tension. Thus, the interfacial Gibbs free energy would be reduced to a relatively lower value towards an equilibrium state, where the spreading of water on the hydrate surface is spontaneous. The spreading of water on hydrate surface leads to a dramatic drop in the interaction force from point II to III, indicating that a relatively strong attractive force (initial interaction force) acted between the droplet and hydrate particle. Along with the instantaneous expansion of the TPC line, the water in the TPC line also forms hydrate due to the high subcooling and the induction (seeding) from the hydrate particle. The original TPC line (see the red line in Fig.3B) sinters on the hydrate particle surface and reduces any further spread of water on the hydrate particle. The attached droplet continues to deform against the hydrate particle surface, thereby increasing the force pushing down on the hydrate particle surface. Meanwhile, hydrate forms along the droplet surface and

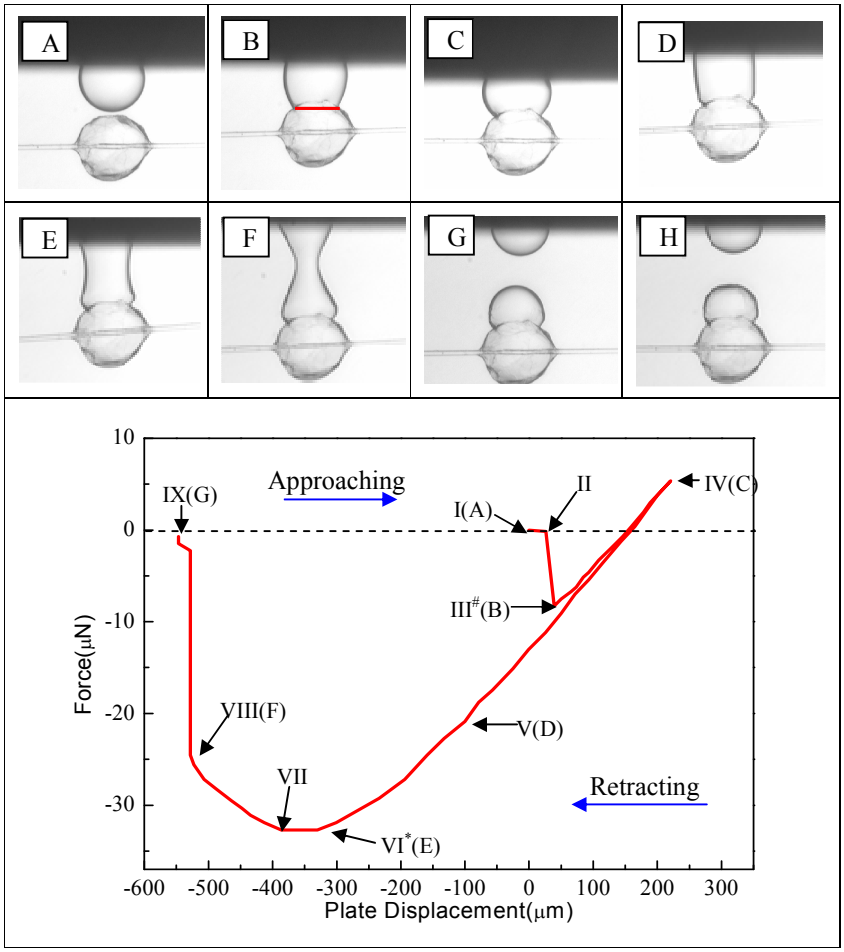

Fig. 3 Typical hydrate particle-droplet interaction force profile (bottom) and corresponding microscope images (top) of a measurement cycle in pure CyC5 at 1.5ºC. III: initial interaction force; IV: preload force; VI: maximum interaction force; VIII: rupture force. III-VIII: t=79 s. Fig. 3H corresponds to the moment when the water left on the hydrate particle was fully covered by a hydrate shell. G-H: t=107 s. The diameter of the glass fiber in the images is 38μm. # represents the initial interaction force, while * suggests the maximum interaction force.

the TPC line moves closer to the aluminum plate. As the aluminum plate reaches point IV, the repulsive force achieves its maximum valve (preload force) and no movement of the original sintering TPC line is observed. It is interesting to note that from points III to IV, the force curve is linear, which indicates the droplet behaves as a spring in this region [25]. As the aluminum plate retracts away from the hydrate particle, the droplet is changed gradually from compression to stretching. Correspondingly, the interaction force shifts from a repulsive force to an attractive force. From the respective microscope image, Fig. 3D，it suggests that the geometry of the region near the hydrate particle-droplet junction has changed significantly due to hydrate formation along the capillary

bridge. From point IV to V, the force curve is again linear, demonstrating that the droplet behaves as a spring at small loading force. However, the slopes of these two linear regions (regions III-IV and IV-V) are slightly different showing the contact angle hysteresis between droplet approach and retraction from the hydrate particle surface [26]. As the aluminum plate is further away from the hydrate particle, the attractive force curve bends from point V to VI due to the large droplet deformation where the behavior of the droplet no longer follows Hooke's law. At point VI, the interaction force reaches the maximum (maximum interaction force/adhesion force) and remains constant until point VII. After the force plateaus at this maximum value (~ -33 μN), the interaction force begins to decrease when the droplet is further stretched from the hydrate particle and a significant necking forms in the capillary bridge (Fig. 3F). Finally, at point VIII, the droplet/liquid bridge breaks at the neck and some amount of water is left on the hydrate particle (Fig. 3G). After the rupture, the liquid water on the plate and hydrate particle become spherical as the system interfacial Gibbs free energy tends to become minimum. The left-hand cantilever sometimes cannot fully return back to the initial position, which is an anomaly of the experimental method at the end of experiment for relatively high force values. It is interesting to note that, during rupture of the capillary bridge, a satellite drop may form as a consequence of this process, which is often observed in the breakup of droplets [27,28]. During the whole retraction period (IV-VIII & C-F), the original sintered junction (where the outer edge of the capillary bridge has sintered to form hydrate) does not move, while the TPC line appears to move (along with further hydrate formation) along the capillary bridge (towards the plate, as determined from the microscope images). For the water left on the hydrate particle (Fig. 3H), hydrate growth continues to span the droplet surface and a hydrate shell covers the droplet within a few minutes due to the high formation rate (high subcooling). The morphology of the new hydrate surface still maintains the shape of the droplet with a slight change in curvature.

To investigate the effect of contact time on hydrate particle-water droplet interaction, the droplet and particle were allowed to rest under constant preload force for 180 s before starting the retracting period. The force profile and

corresponding images are shown in Fig. 4. For the approaching process (point I to IV), as expected, the force profile shows similar behavior as shown in Fig. 3. During the extended contact time, the force increases from point IV to point V due to hydrate growth on the droplet surface which changes the curvature of the original droplet slightly. For the retracting process, the interaction force profile is siginificantly different from Fig. 3: (i) before the interaction force reaches the maximum, the retracting force curve is approximately linear (point V to point VI); (ii) the liquid bridge breaks (point VII) just as the interaction (attractive) force reaches a maximum value (point VI). This maximum interaction force is approximately equivalent to the rupture force of the capillary

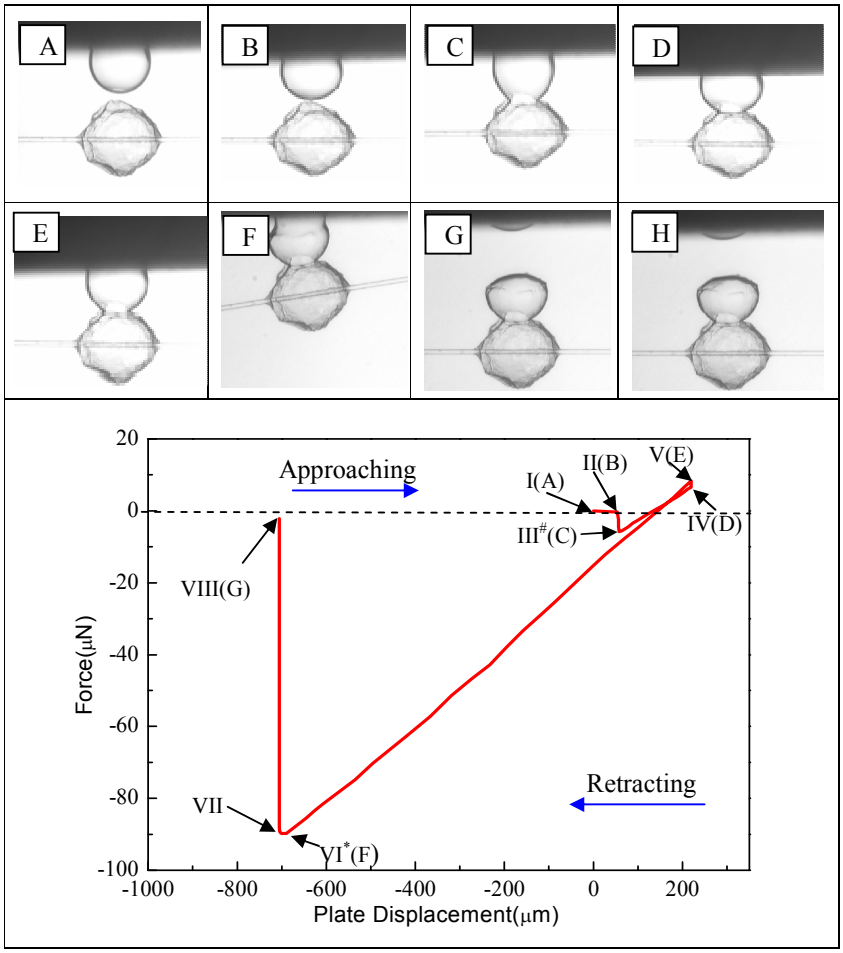

Fig. 4 Typical hydrate particle-droplet interaction force profile (bottom), and corresponding microscope images (top) of a measurement cycle in pure CyC5 at 1.5 ºC. III: initial interaction force; IV: preload force; IV-V: The droplet and particle are allowed to rest under constant preload force for 180 s (extended contact time) before retracting; VI: maximum interaction force; VII: rupture force. III-VII: t=275 s. Fig. 4H shows the hydrate morphology when the water left on the hydrate particle was fully covered by a hydrate shell. G-H: t=51 s.

bridge. In addition, due to more water converting to hydrate during the measurement, only a small amount of water is left on the aluminum plate after the rupture. The difference can be explained by, during the extended contact time, hydrate growth spans the surface of the droplet and a large proportion of the droplet is surrounded by a hydrate shell. Consequently, the water volume between the aluminum plate and the new TPC line is much smaller. The respective microscope images suggest that in the retracting portion (point V to VII), the deformation of the liquid bridge is quite small due to the much smaller liquid volume, therefore leading to: (i) the nearly constant spring coefficient of the liquid bridge and subsequently the approximately linear force profile for IV to VI; (ii) the force profile for VI to VII is so sharp compared to the gradual curve in Fig. 3 from VI to VIII. Although the initial sizes of the droplet and hydrate particle in Figs. 3 and 4 are similar, and the preload forces also show insignificant differences (~ 1.1μN), the maximum interaction force in Fig. 4 (~ - 90 μN) is much larger than that in Fig. 3 (~ - 33 μN).

From the microscope images in Figs. 3 and 4, the interaction between the droplet and hydrate particle are dominated by the capillary bridge/force. It is expected that the hydrate shell can form around the whole droplet surface with a long enough contact time. In this case, the tensile strength of hydrate will govern the interaction force [9].

Effect of temperature/subcooling

The force profile and respective microscope images at a temperature of 7.0 ºC (i.e. at a subcooling of 0.7 ºC, see Fig. S1) are shown in Fig. 5. The aluminum plate approaches the hydrate particle from point I to II at which the liquid film between the surfaces ruptures. Subsequently, the hydrate particle suddenly “jumps” towards the droplet (point III) and the three phase contact (TPC) line forms. Compared to the previous measurements (Figs. 3 and 4), the hydrate formation rate is much lower due to the lower subcooling/driving force. The water-hydrate interaction behavior here is similar to that between water and hydrophilic solid particles (e.g. glass ball, powder) which have

been widely investigated [25]. The attached droplet continues to deform against the lower hydrate particle surface between hydrate and CyC5. When the contact angle is around the receding value [25], the TPC line starts to move, forming a flat region in the force profile (point IV to V). The further movement of the TPC line leads to a larger contact area between the droplet and hydrate surface. During the retracting period, the interaction force profile is similar to that in Fig. 3. Figs. 5A to G, suggest that there is no visible hydrate formation during the measurement. After the breakage of the liquid bridge, water remaining on the hydrate particle eventually converts to hydrate. Due to the lower driving force, the hydrate formation rate is quite slow and more than one hour is needed to

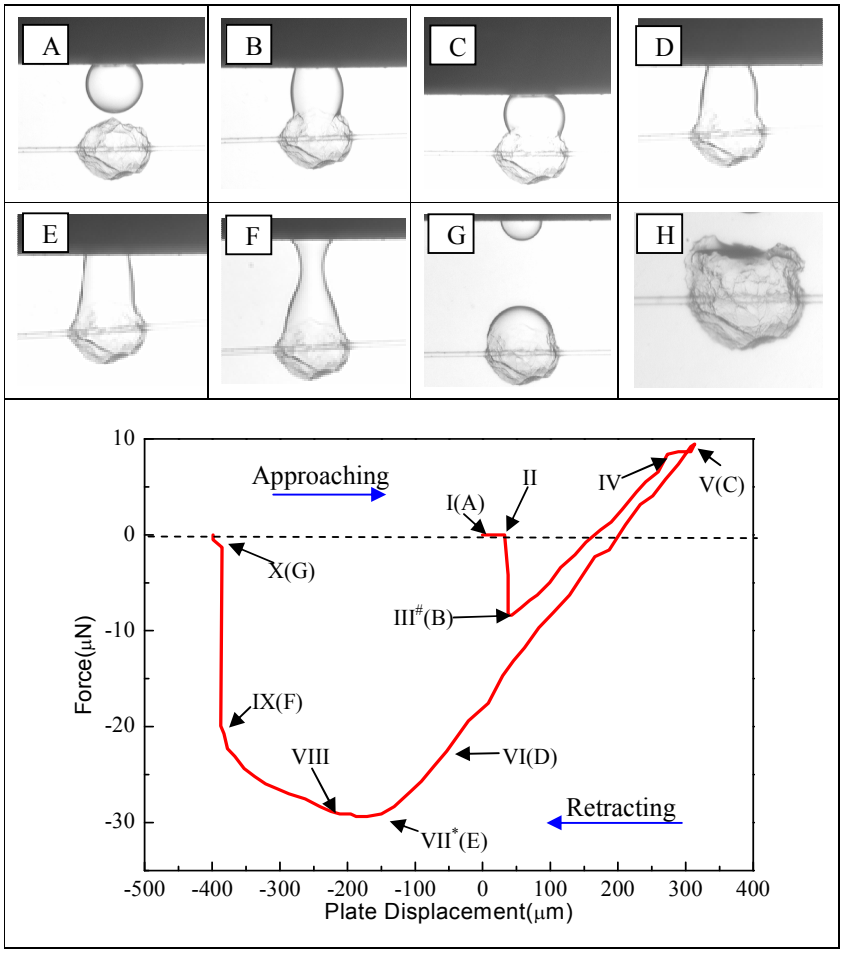

Fig. 5 Typical hydrate particle-droplet interaction force profile (bottom), and corresponding microscope images (top) of a measurement cycle in pure CyC5 at 7 ºC. III: initial interaction force; IV-V: TPC line movement; V: preload force; VII: maximum interaction force; IX: rupture force; III-IX: t=89 s. Fig. 5H is at higher magnification to show the different hydrate formation morphologies. G-H: t=4467 s.

convert the remaining water into hydrate. Fig. 5H indicates that the hydrate formation process/morphology at lower driving force (see Fig. S2) is significantly different from that at higher driving force. At higher driving force (Fig. 3), hydrate growth begins at the TPC line and spans along the droplet surface. Finally, the droplet is surrounded by a hydrate shell whose shape is close to the original shape of the droplet (despite the slight change in curvature). At lower driving force, hydrate growth also begins at the TPC line. However, the hydrate morphology changes, and eventually an irregular basin-like geometry forms on the original hydrate particle surface (see Fig. 5H and Fig. S2). These distinct hydrate morphologies were commonly observed in the repeat experiments (Fig. S3). It is expected that the contact time will have a less significant effect on the force curve due to the much lower hydrate formation rate at this low subcooling (as indicated in Fig. S4).

The hydrate particle-water droplet interaction measurements at different subcoolings suggest that at higher subcooling, the higher hydrate formation rate leads to more water being converted to hydrate during the measurement, which will increase the maximum interaction force (see Fig. 8) and consequently the particle agglomerate size. Larger agglomerate sizes can lead to higher slurry viscosity [29,30].

Effect of mineral oil

Fig. 6 shows the force curve and respective microscope images of the hydrate-droplet interaction in a mixture of CyC5 and mineral oil 70T at 1.5 ºC. The mass ratio of CyC5 to mineral oil 70T is 1:1. Compared with the hydrate-droplet interaction in pure CyC5 at 1.5ºC, the addition of mineral oil decreased the hydrate formation rate. The reason can be explained by the reduction in subcooling (ΔT_{sub} = ~5 ºC) due to the addition of mineral oil (see Fig. S1). According to the microscope images (Fig. 6A-G), no visible hydrate formation was observed during the approaching-retracting processes. The lower hydrate formation rate results in the hydrate-droplet interaction behavior being similar to that in pure CyC5 at lower subcooling (e.g. Fig. 5). It is interesting to note that, although the lower hydrate formation rates of the CyC5/mineral oil mixture at lower temperature (1.5ºC) and pure CyC5 at

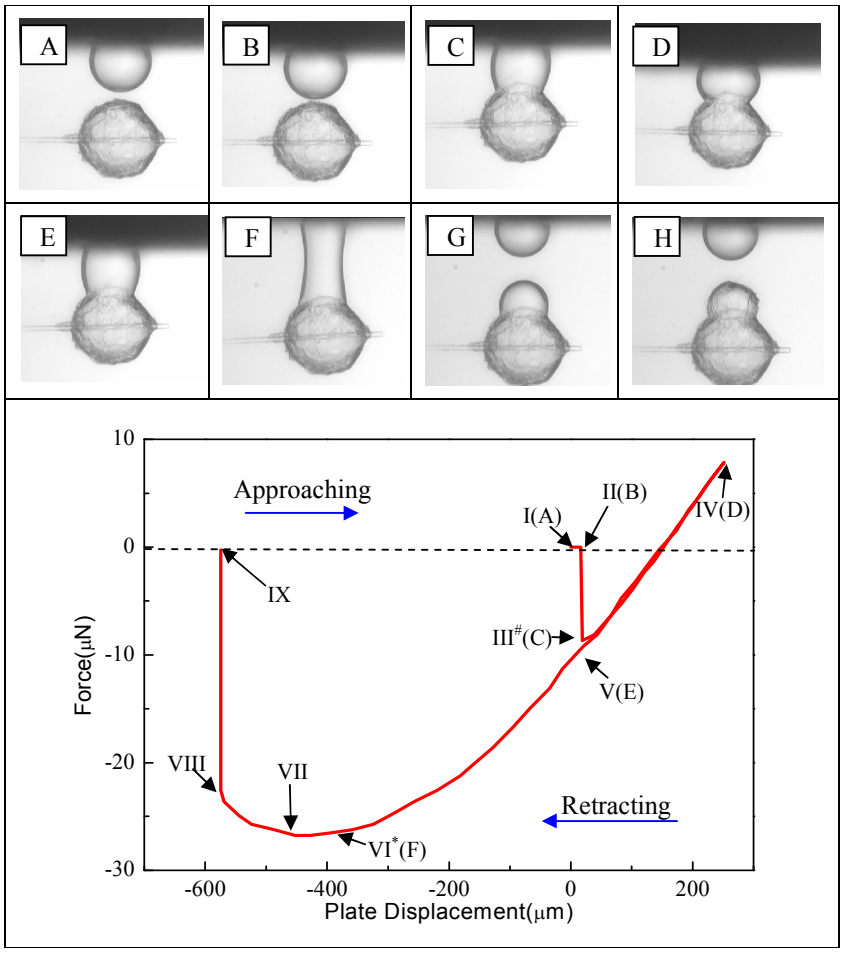

Fig. 6 Typical hydrate particle-droplet interaction force profile (bottom), and corresponding microscope images (top) of a measurement cycle in a mixture of CyC5 and mineral oil 70T (mass ratio 1:1) at 1.5ºC. III: initial interaction force; IV: preload force; VI: maximum interaction force; VIII: rupture force. III-VIII: t=87 s. Fig. 6H shows the hydrate morphology when the water left on the hydrate particle was fully covered by a hydrate shell. G-H: t=726 s.

higher temperature (7 ºC) lead to similar hydrate-droplet interaction behaviors, the hydrate formation morphology on the hydrate particle is different. As shown in Fig. 6H, hydrate formation occurs along the droplet surface, which is similar with that in Fig. 3.

Effect of Span 80

Span 80 is a common water-in-oil type surfactant, and its effects on hydrate growth morphology and hydrate particle cohesion force have been reported in previous work [3,31]. Fig. 7 shows the two test cycles for the addition of 1 wt.% Span 80 in CyC5, which produces a significantly different particle-droplet interaction behavior from

that without Span 80. It should be noted that due to the addition of Span 80, the method for generating a drop on the aluminum plate could not be used (since the drop would not remain on the surface). Instead, a brass surface with an epoxy coating (Epoxy-A) was used to hold the droplet, and the droplet was transferred from the glass fiber to the epoxy coated surface in air and then was immersed in the cell bath to perform the measurement. As shown in Fig. 7, the addition of Span 80 induced a morphological change on the hydrate surface, where hair-like extrusions extended from the surface into the bulk phase. Delgado-Linares [3] and Karanjkar [31] have reported a similar phenomenon. Karanjkar suggested that the addition of Span 80 after formation of a hydrate shell appears

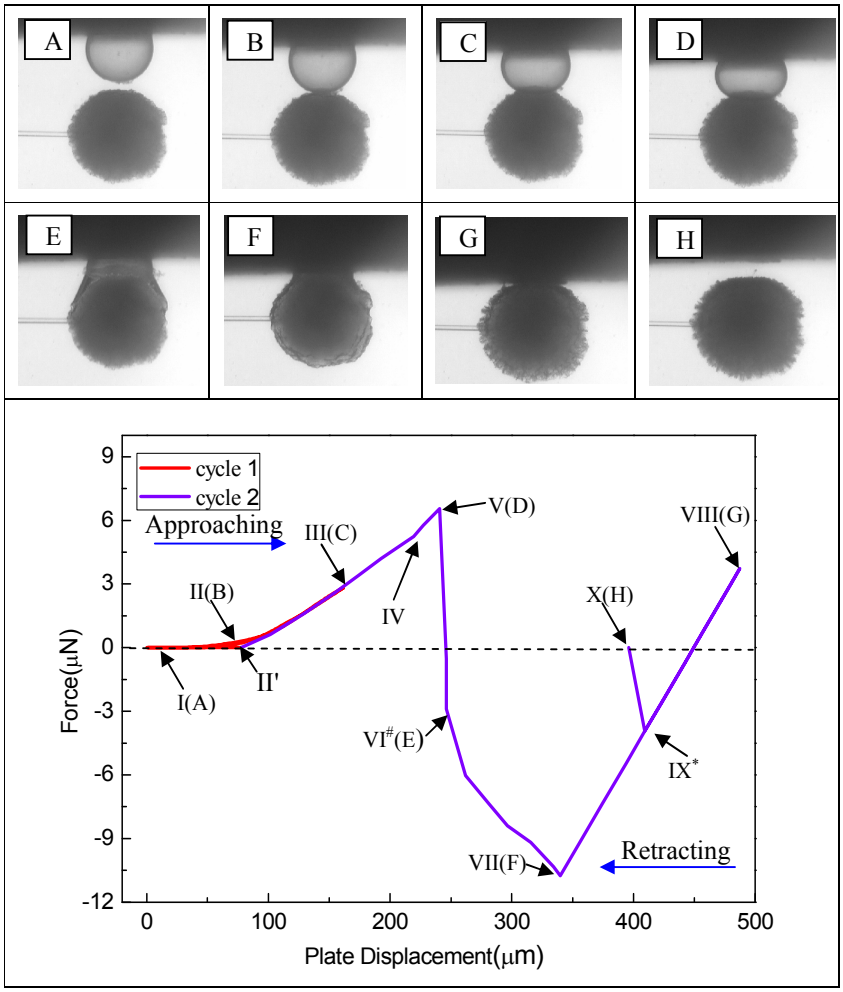

Fig. 7 Typical hydrate particle-droplet interaction force profile (bottom), and corresponding microscope images (top) of two measurement cycles in CyC5 with 1 wt.% Span80 at 1.5 ºC. II': droplet-hydrate particle initial contact (cycle 2); V: droplet rupture; VI: initial interaction force; VIII: preload force; IX: rupture force. II'-IX: t=86 s.

to weaken junctions between surface crystals. Internal water then flows out to contact the external CyC5, leading to rapid hydrate formation and consequently an irregular surface growth, more details can be found in reference 31. In addition, due to the concentration (1 wt.%) of the Span 80 in CyC5 being much higher than the critical micelle concentration, 0.04 wt.% [24], inverse micelles formed and could lead to the formation of tiny droplets. The tiny droplets could accumulate/aggregate on the large droplet surface to make the original transparent droplet appear dark. The droplet begins to approach the hydrate particle at point I and contacts the particle surface at point II. Unlike the previous measurements (Figs. 3-6), the droplet interface does not break once the two surfaces contact each other. Span 80 has distinct hydrophilic and hydrophobic groups, and the hydrophilic head can bind to the hydrate surface while the hydrophobic tails can extend into the continuous bulk phase. On the other hand, adsorption of Span 80 on the water droplet surface can form a layer, which can increase the strength of the droplet surface. Therefore, the droplet does not rupture at the initial contact position. As the plate continues to approach the hydrate particle, the droplet is compressed against the particle surface, increasing the force pushing on the particle. At point III, the approach process is finished and the retracting portion began. The retracting force curve is almost entirely coincident with the approaching force curve. When the plate returns to the original position, there is no measurable interaction force between the droplet and hydrate particle. Similar with the previous measurements, the force curve also presents a linear region between points II and III. For the second measurement, at the beginning the force curve is superimposed on the first cycle trace. As the droplet continues to deform against the hydrate particle, the droplet no longer behaves as a spring and the force curve begins to increase to point IV. With the further increase in repulsive force (due to an increased applied contact force), the droplet surface becomes unstable and ruptures at point V. The hydrate particle is pulled into the droplet, corresponding to a dramatic drop in the interaction force from point V to VI. Meanwhile, the water from the liquid bridge spreads over the entire hydrate particle surface and rapidly converts into hydrate due to the larger interface between water and CyC5, which was not observed in pure cyclopentane. The reason can be explained by the fact that in pure

CyC5, the water-CyC5 interfacial tension is high (~48.7 mN/m[24]), further spreading of water on the hydrate surface after the initial contact may result in an increase in system interfacial Gibbs free energy due to the increase of the water-CyC5 interfacial area. Therefore, further spreading of water will not occur without providing additional energy/force. However, the addition of Span 80 in cyclopentane can significantly reduce the water-CyC5 interfacial tension (~1 mN/m at the critical micelle concentration), thus causing the water to spread over the entire hydrate particle spontaneously [24]. As more water transfers to the hydrate particle surface and forms hydrate, the water amount in the liquid bridge decreases and the particle is engulfed into the droplet gradually (point VI to point VII). Finally, the hydrate particle comes into direct contact with the plate at point VII. As the plate continues to push the particle from point VII to point VIII, the cantilever deflects in proportion, exhibiting a linear profile due to the hydrate particle interacting with the plate. Meanwhile, the residual free water on the hydrate particle continues to form hydrate rapidly, resulting in the significant change on the surface morphology and hydrate particle size (Fig. 7G). As the plate retracts from the particle, the retracting force curve is entirely coincidence with the approaching force curve. At point IX, the particle breaks away from the plate and returns to the original position (point X). It should be noted that, in Fig. 7, although the hydrate particle contacts the plate, the hydrate does not sinter on the plate, therefore, it is easy to separate them. However, in the case of the hydrate particle sintering on the plate (repeat experiment), the interaction force will be extremely large, which will be beyond the range of this equipment (see Fig. S5).

The hydrate particle-droplet interaction behavior with Span 80, suggests that: (i) Span 80 adsorbs on hydrate particle surfaces, resulting in changes in hydrate morphology. Meanwhile, the presence of Span 80 on both the hydrate and water interfaces can form adsorption layers, which can have relatively strong mechanical strength. The interfacial layers can render the interfaces more stable versus coalescence, thereby hindering the formation of water bridges. This suggests that Span 80 can be effective in preventing hydrate agglomeration, as reported previously by Huo et al.[32]; (ii) when the contact force exceeds the strength of the interface, the droplet will rupture

and the water spreads on the whole hydrate particle surface, and at higher subcooling the water will form hydrate rapidly.

Effect of contact area

It should be noted that the hydrate particle is not an ideal sphere, and the geometry and roughness of the particle will show some differences. This will affect the contact area between the water droplet and hydrate particle, and consequently affects the interaction force between them.

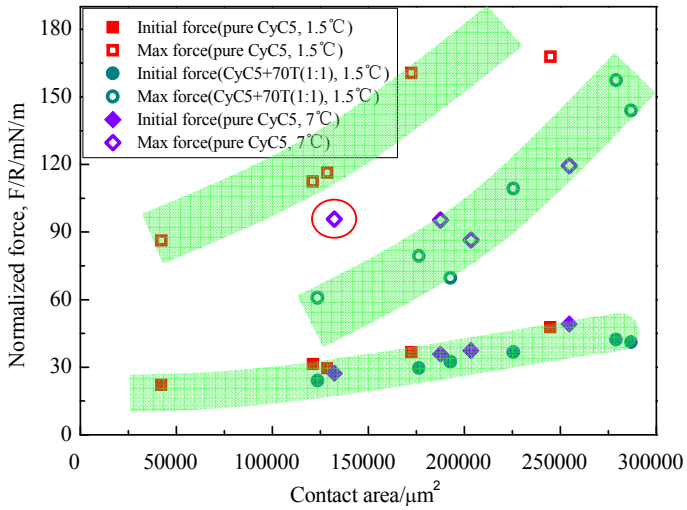

Fig. 8 Initial interaction force/ maximum interaction force vs. contact area. The normalized force refers to the interaction force divided by the radius of the hydrate particle. (The repeatability of these measurements is illustrated in Fig. S7).

Fig. 8 shows the effect of contact area on the hydrate particle and droplet interaction forces, the initial interaction force, and the maximum interaction force. The contact area refers to the circular area of the initial three phase contact line (see Fig. S6). The coefficient of variation (i.e. standard deviation/mean×100%) of the data is less than

~4% (see Fig. S7). The variation could be due to several reasons. In this work, the plate movement speed is manually controlled, so the inevitable fluctuation of the movement speed could affect the measured force. As mentioned, a satellite drop may be generated during the rupture of the liquid bridge, which will reduce the water volume in the following repeat measurement and result in some variation in the force. In addition, some errors can also arise during the force analysis using the image J processing software.

According to the microscope images shown in Figures 3, 5, 6, the capillary force dominates the hydrate particle-droplet interaction. The pendular liquid bridge model (see Fig. 9) can be proposed for describing the interaction behavior [33]. The corresponding capillary force F, is given by [25,33]

$$F = \pi R_p^2 \sin^2 \varphi_p \Delta P - 2\pi R_p \sin \varphi_p \gamma_{hw} \sin\left(\varphi_p + \theta_p\right) \quad (1)$$

Where R_p is the radius of hydrate particle, φ_p is the half filling angle of the hydrate particle-capillary bridge contact as shown in Fig. 9. γ_{hw} is the water-hydrocarbon interfacial tension, θ_p is the contact angle of the liquid bridge on particle surface, and ΔP is Laplace pressure drop across the hydrocarbon/water interface which can be presented as [34]

$$\frac{\Delta P}{\gamma_{hw}} = \frac{1}{y\left(1+y'^2\right)^{1/2}} - \frac{y''}{\left(1+y'^2\right)^{3/2}} \quad (2)$$

Where y' and y'' are the first and second derivatives of the liquid bridge profile described by the function $y(x)$.

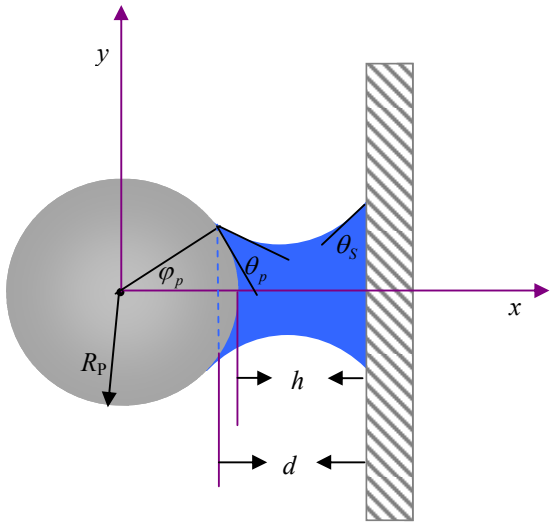

Fig. 9 Illustration of a pendular liquid bridge between a sphere and flat plate. More details can be found in reference [33].

As shown in Fig. 8, for three data sets, both the initial interaction force and the maximum interaction force increase with the contact area, which is in agreement with eq. (1). Furthermore, the initial interaction forces are nearly equal with similar contact area. According to eqs. (1) and (2), the interfacial tension (γ_{hw}) will have a significant effect on the interaction force. For pure CyC5, the water-liquid CyC5 interfacial tension is about 48.7 mN/m [24], while the interfacial tension between water and mineral oil 70T is about 50 mN/m [2]. Therefore, the water-liquid CyC5 interfacial tension and water-liquid CyC5+mineral oil 70T (1:1) interfacial tension should be similar, consequently resulting in the similar initial interaction force with similar contact area. For the CyC5+mineral oil 70T mixture at 1.5 ºC and pure CyC5 at 7 ºC, there is no visual hydrate formation during the measurement, therefore the maximum interaction forces with the same contact area are similar, this can be also explained by their similar interfacial tension. However, for the pure CyC5 at 1.5 ºC, the maximum interaction force is much larger than the former two data sets despite the same interfacial tension. This difference can be due

to the higher hydrate formation rate in this condition; the increased contact time (Fig. 4) also confirms this hypothesis. Song et al.[15] also suggested that hydrate formation would increase the interaction force dramatically. It is interesting to note that, for pure CyC5 at lower subcooling (0.7 ºC), there is an anomalous point (marked with a red circle). This point corresponds to Fig. 5 where the images and interaction force curve suggest that the original three phase contact line moves and increases the contact area during the measurement, resulting in the larger maximum interaction force.

Compared with the hydrate particle-particle cohesion force (4.3±0.4 mN/m at 3 ºC [9]) in CyC5, the hydrate particle-droplet adhesion force/maximum interaction force (without Span 80) is at least an order of magnitude larger, and the force increases as more water converts to hydrate. A similar qualitative conclusion was also suggested by Aspenes et al.[17]. Given the hydrate-droplet interactions can occur at the early stage of agglomeration, it can be expected that the unconverted liquid droplets will interact with the hydrate particles and form larger-scale agglomerates due to the strong interaction force between them. With the unconverted water forming hydrate gradually, the hydrate particles/droplets in the agglomerate will sinter together. Once all the water is covered by a hydrate shell, the hydrate–hydrate cohesion force will dominate. However, since the hydrate-hydrate cohesion force is much lower than the hydrate-water droplet force, the agglomerates formed in the early stage are expected to be dominant in this condition. For the system with Span 80: if the external force can break the interface between the droplet and hydrate particle, the hydrate-droplet adhesion force will dominate, which is similar to the systems without Span 80; while if the external force is not large enough to break the interface, the hydrate-droplet interaction force will be much smaller, and the droplets will not interact with the hydrate particles to form large agglomerates.

Conclusions

The hydrate-droplet interaction force can play a critical role in the early stage of hydrate agglomeration. With a

unique micromechanical force apparatus, direct measurements of the hydrate-droplet interaction were performed. The effect of contact time, temperature/subcooling, contact area, and the addition of mineral oil 70T and Span 80 on the water droplet–hydrate particle interaction force were investigated. The results indicate that longer contact time and higher subcooling lead to more water converting to hydrate during the measurements, which can increase the hydrate particle-water droplet interaction force significantly. The addition of mineral oil 70T will reduce the hydrate formation rate, resulting in a decrease in the hydrate-droplet adhesion force. The interaction force also increases with hydrate-water contact area. The adsorption of Span 80 on the droplet and hydrate surface can render the interfaces stable, and the interaction behavior depends on the contact force. The hydrate particle-water droplet adhesion forces are at least an order of magnitude larger than the hydrate-hydrate cohesion force (4.3 mN/m). The observations and quantitative analysis in this study can help to improve the current understanding and model development on hydrate agglomeration, which could lead to better strategies to control this process.

Acknowledgements

The authors acknowledge support from the CSM Hydrate Consortium. Chenwei Liu also acknowledges the support from the Program for Changjiang Scholars and Innovative Research Team in University (IRT1294) and "the Fundamental Research Funds for the Central Universities" (Grant No. 14CX06026A).

References

1 E. D. Sloan and C. A. Koh, Clathrate Hydrates of Natural Gases. 3rd Ed., CRC Press-Taylor & Francis Group, Boca Raton, FL. 2007.

2 J. D. Smith, A. J. Meuler, H. L. Bralower, R. Venkatesan, S. Subramanian, R. E. Cohen, G. H. McKinley and K.K. Varansi, Phys. Chem. Chem. Phys., 2012, 14, 6013–6020.

3 J. G. Delgado-Linares, A.A. Majid, E.D. Sloan, C.A. Koh and A.K. Sum, Energy & Fuels, 2013, 27, 4564–4573.

4 D.J. Turner, Ph.D. Thesis, Colorado School of Mines, Golden, CO. 2005.

5 A Fidel-Dufour, PhD thesis, Ecole Nationale Superieure des Mines de St-Etienne, St-Etienne, France, 2004.

6 R. M. Dhenge K. Washino, J. J. Cartwright, M. J. Houslow and A. D. Salman, Powder Technology, 2013, 238, 77–90.

7 B.J. Ennis and J. D. Litster, Particle size enlargement, in: R. Perry, D. Green Eds., Perry's Chemical Engineers' Handbook, 7th Ed., McGraw-Hill, New York, 1997.

8 S. M. Ivesona, J. D. Litster, K. Hapgood and B. J. Ennis, Powder Technology, 2001,117, 3–39.

9 Z. M. Aman, E. P. Brown, E. D. Sloan, A. K. Sum and C. A. Koh, Phys. Chem. Chem. Phys., 2011, 19796–19806.

10 S. Yang, D. Kleehammer, Z. Huo, J. E Dendy Sloan and K. Miller, J. Colloid Interface Sci., 2004, 277, 335–341.

11 C. Taylor, L. Dieker, K. Miller, C. Koh and J. E. Dendy Sloan, J. Colloid Interface Sci., 2007, 306, 255–261.

12 L. E. Dieker, Z. M. Aman, N. C. George, A. K. Sum, E. D. Sloan and C. A. Koh, Energy Fuels, 2009, 23, 5966–5971.

13 B. R. Lee, C.A. Koh and A.K. Sum, Industrial & Engineering Chemistry Research, 2014, 53,18189–18193.

14 J.H. Song, A. Couzis and J.W. Lee, Langmuir, 2010, 26, 9187–9190.

15 J.H. Song, A. Couzis and J.W. Lee, Langmuir, 2010, 26, 18119–18124.

16 M.J. Cha, A. Couzis and J.W. Lee, Langmuir, 2013, 29, 5793–5800.

17 G. Aspenes, L.E. Dieker, Z. M. Aman, S. Hoiland, A.K. Sum, C.A. Koh and E.D. Sloan, Journal of colloid and interface science, 2010, 343, 529–536.

18 Z.M. Aman, E.D. Sloan, A. K. Sum and C.A. Koh, Phys.Chem.Chem.Phys., 2014,16, 25121–25128.

19 M. L. Fielden, R. A. Hayes and J. Ralston, Langmuir, 1996, 12, 3721–3727.

20 N. Ishida, Colloids and surfaces A: Physicochem. Eng. Aspects, 2007, 300, 293–299.

21 B.A. Snyder, D.E. Aston and J.C. Berg, Langmuir, 1997, 13, 590–593.

22 L. Jiang, M. Krasowska, D. Fornasiero, P. Koh and J. Ralston, Phys. Chem. Chem. Phys., 2010, 12, 14527–14533.

23 Z. M. Aman, K. Olcott, K. Pfeiffer, E. D. Sloan, A. K. Sum, and C. A. Koh, Langmuir, 2013, 29, 2676–2682.

24 P. U. Karanjkar, Ph. D thesis. CITY UNIVERSITY OF NEW YORK. 2012.

25 L.X. Wang, D. Sharp, J. Masliyah and Z.H. Xu, Langmuir, 2013, 29, 3594–3603.

26 M. Preuss and H. Butt, Langmuir, 1998, 14, 3164–3174.

27 X. Pepin, D. Rossetti, S.M. Iveson and S.J.R. Simons, Journal of colloid and interface science, 2000, 232, 289–297.

28 J.F. Padday, G. Petre, C.G. Rusu, J. Gamero and G. Wozniak, J. Fluid. Mech., 1997, 352, 177–204.

29 R. Wessel and R. C. Ball, Physical Review A, 1992, 46, 3008–3011.

30 E.B. Webb, C. A. Koh and M.W. Liberatore, Langmuir, 2013, 29, 10997–11004.

31 P. U. Karanjkar, J.W. Lee and J. F. Morris, Crystal growth and design, 2012, 12, 3817–3824.

32 Z. Huo, E. Freer, M. Lamar, B. Sannigrahi, D. M. Knauss and E.D. Sloan, Chem Eng Sci., 2001, 56, 4979–4991.

33 C. W. Liu, Ph. D thesis. China University of Petroleum. 2014.

34 D. Rossetti, X. Pepin and S.J.R. Simons, Journal of colloid and interface science, 2003, 261, 161–169.